Available online at www.sciencedirect.com

ScienceDirect

Procedia Structural Integrity 2 (2016) 1983–1990

Structural Integrity Procedia

www.elsevier.com/locate/procedia

21st European Conference on Fracture, ECF21, 20-24 June 2016, Catania, Italy

A coupled FFM model to interpret fracture toughness values for brittle materials

Donato Firrao[a], Paolo Matteis[a], Alberto Sapora[b]*, Pietro Cornetti[b], Alberto Carpinteri[b]

[a]*Department of Applied Science and Technology, Politecnico di Torino, Corso Duca degli Abruzzi 24, 10129 Torino, Italy*

[b]*Department of Structural, Geotechnical and Building Engineering, Politecnico di Torino, Corso Duca degli Abruzzi 24, 10129 Torino, Italy*

Abstract

Around 1970 quenching AISI 4340 steel from 1200 °C was discovered to lead to much higher fracture toughness, in the as quenched state, than by conventional austenitizing at 870 °C. Further researches have ascertained that the apparent toughness increase is limited to fracture toughness tests, whereas Charpy-V impact tests do not show any betterment due to high temperature austenitizing, in respect to conventional heat-treating. Various explanations of these contradicting results were given on the basis of the then existing theories. The puzzling phenomenon is here interpreted by means of Finite Fracture Mechanics theories, based on the contemporaneous fulfilment of a stress requirement and the energy balance.

Keywords: HTA steel, CTA steel, notch radius, austenitic grain size, Finite Fracture Mechanics

1. Introduction

High Temperature Austenitizing (HTA) of steels, i.e. austenitizing at temperatures well above the A_{c3} critical point, has been historically considered detrimental since it promotes large austenitic grain growth and in turn the raise of the ductile-to-brittle transition temperature, as measured by Charpy-V type specimens, in respect to conventionally austenitized (CTA) steels. Since 1969 in the then USSR and 1972 in the USA, a scientific movement towards the adoption of HTA was born, based on a spectacular raise of fracture toughness of as-quenched low alloy high strength steels upon increasing the austenitizing temperature (Bashchenko and Mel'nichenko 1969, Zackay et al.

* Corresponding author. Tel.: +39-011-0904911; fax:+39-011-0904989.
E-mail address: alberto.sapora@polito.it

10.1016/j.prostr.2016.06.249

1972). On the other hand, Charpy-V impact tests still confirmed that austenitization at the usual (A_{c3} + 50 °C) temperature yielded larger absorbed energy values than by adopting HTA (Lai et al. 1974, Ritchie et al. 1976, Roberti et al. 1978). The above described contradictory phenomenon of the different influence of HTA and CTA on fracture properties of pre-cracked and round notch samples was further confirmed by slow bend tests (Firrao et al. 1982) on as-quenched AISI 4340 steel Charpy V-type bars with varying notch root radii ρ, austenitized at low and high temperature and quenched in oil. A step quenching procedure from 1200°C was adopted to avoid quench cracks at the root of the notch if a direct quench from the high temperature had been used.

By mid eighties HTA was abandoned on the assumption that no industrial application could be associated with it. Nowadays light weight design calls for the use of high strength fasteners with tensile strengths well above those foreseen by the 12.9 property class (ISO 898-1 standard). Whereas the requirement has opened again explorations into high strength low alloy steels quenched and tempered at low temperatures, the adoption of HTA might be again usefully revisited.

In the present work the coupled Finite Fracture Mechanics (FFM) criterion (Carpinteri et al. 2012, Sapora et al. 2015) will be applied to estimate the apparent fracture toughness as a function of the notch radius for the HTA and CTA steel specimens tested in (Firrao et al. 1982). The approach is based on the contemporaneous fulfilment of a stress requirement and the energy balance, the latter being implemented on the basis of a recently proposed analytical expression for the stress intensity factor (Sapora et al. 2014). Only two material parameters are involved in the analysis, namely the tensile strength σ_u and the fracture toughness K_{Ic}. FFM involves a critical distance which results to be a structural parameter, depending on the material properties and the notch radius. The correlation between this length and the microstructure of austenized steels will conclude the paper.

2. Fracture modes of HTA and CTA steel samples

Both HTA and CTA K_{Ic} specimens failed by brittle intergranular mode. Different fracture morphologies were instead encountered while examining rupture surfaces of round V-notch samples. All the HTA samples failed by a predominantly brittle intergranular fracture, irrespective of the ρ value. Instead, CTA samples with a sufficiently large ρ showed a peculiar fracture path with the formation of a continuous shear lip emanating at some distance from the notch centerline and then traveling along a logarithmic spiral to the region of the sample minimum section (Fig. 1) (Firrao et al. 1980). Larger and larger shear lips were detected as the ρ value increased. These features were associated with a slip line field forming at the root of the notch under the applied slow bending loads. Critical J-integral values at increasing ρ's were found in direct correspondence with the length of the arc of slip lines traveled by the crack during the plastic instability prior to final fracture along the sample center line. Similar behaviors have been found in round notch samples fabricated with other types of alloy steels with low strain hardening exponents (Firrao and Ugues 2005).

To further investigate into the role of the purity of steels and of the prior austenitic grain size, blunt notch samples from two more different heats of AISI 4340 steels were fabricated and slow bend tested in the as-quenched condition, both from HTA or CTA. Thus, alongside the heat previously tested (A Steel), the heats listed in Table 1 were sampled (Firrao et al. 2015).

Table 1: Chemical composition of sampled heats of AISI 4340 steel (wt pct).

	C	Mn	Ni	Cr	Mo	Si	P	S
A	0.40	0.75	1.74	0.81	0.23	0.26	0.019	0.015
B	0.41	0.75	1.69	0.78	0.24	0.27	0.016	0.015
C	0.41	0.82	1.80	0.85	0.26	0.22	0.009	0.003

A and B steels were fabricated by Electric Arc Furnace, whereas C steel was further Vacuum Arc Remelted (VAR) to reduce P and S contents. Although A and B steels have a very similar compositions, the inclusion type and distribution were quite different; in A steel it was possible to recognize only elongated sulfides, whereas in B steel thin sulfides were accompanied by a few large round inclusions, identified as silicon aluminates. C steel had a very limited amount of slightly elongated sulfides and widely spaced round inclusions. For all the steels, HTA resulted in

lower values of the ultimate tensile strength and elongation to fracture in respect to CTA and in a negligible (A and B steels) or small variation (C steel) of the yield strength.

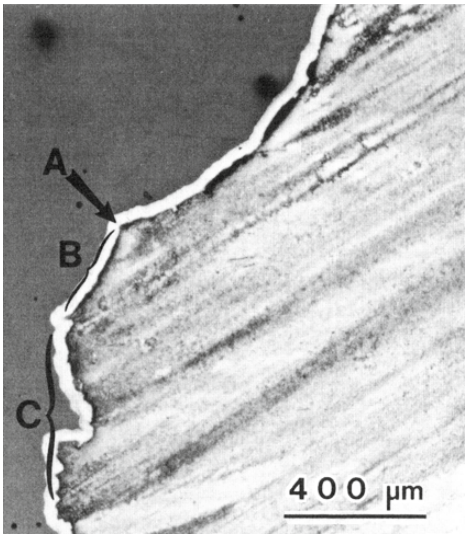

Fig. 1. Fracture path in as-quenched notched specimens austenitized at 870 °C (polished cross section after coating): initiation (A), propagation along a slip surface (B), and final fracture along the minimum section region (C).

3. Finite Fracture Mechanics

The coupled FFM criterion is based on the hypothesis of a finite crack advancement l_c and assumes the contemporaneous fulfilment of two conditions (Sapora et al. 2015). Let us refer to the coordinate system displayed in Fig. 2 for a U-notch geometry. The former condition requires that the average stress $\sigma_y(x)$ upon the critical crack advancement l_c is equal the material tensile strength σ_u.:

$$\int_0^{l_c} \sigma_y(x)\,\mathrm{d}x = \sigma_u\, l_c \tag{1}$$

The latter one ensures that the energy available for a crack length increment l_c (involving the integration of the crack driving force over such a length) coincides with the energy necessary to create the new fracture surfaces. By means of Irwin's formula, this condition can be expressed as:

$$\int_0^{l_c} K_I^2(a)\,\mathrm{d}a = K_{Ic}^2\, l_c \tag{2}$$

$K_I(a)$ being the stress intensity factor (SIF) related to a crack of length a stemming from the notch root (Fig. 2). A system of two equations (1) and (2) in two unknowns (the critical crack advancement l_c and the failure load, implicitly embedded in the stress field and SIF functions) is thus obtained.

By assuming that the notch tip radius ρ is sufficiently small with respect to the notch depth, the stress field along the notch bisector could be approximated by means of Creager-Paris' expression ($x < \rho/2$):

$$\sigma_y(x) = \frac{2K_I^U}{\sqrt{\pi}} \frac{x+\rho}{(2x+\rho)^{3/2}} \tag{3}$$

where K_I^U is the apparent SIF (Glinka 1985).

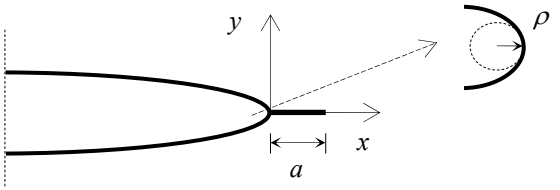

Fig. 2. U-notch geometry with Cartesian system and a crack of length *a* stemming from the notch root.

On the other hand, let us consider a crack of length *a* stemming from the U-notch root (Fig. 1). As far as the notch depth is sufficiently large with respect to *a*, the following SIF function was proposed (Sapora et al. 2014),

$$K_I(a) = \frac{K_I^U}{\left\{1+\left[\frac{\rho}{5a}\right]^m\right\}^{\frac{1}{2m}}} \tag{4}$$

with m=1.82. Note that the parameter m was fitted to improve the predictions obtained by carrying out an *ad hoc* finite element analysis (Sapora et al. 2014): Eq. (4) fulfils the asymptotic limits of very short and very long (but still small in respect to the notch depth) cracks, providing errors below 1%, for $0 \le a/\rho \le 10$. For m=1 in Eq. (4) we have:

$$K_I(a) = \frac{K_I^U}{\sqrt{1+\frac{\rho}{5a}}} = 2.24\sqrt{\frac{a}{\rho+5a}}K_I^U \tag{5}$$

which coincides with the relationship for an elliptical hole (Lukas 1987) when the minor axis to major axis length ratio tends to zero, the only difference being the factor 5 replacing the Lukas' approximation factor 4.5.

By inserting Eqs.(3) and (4) into Eqs.(1) and (2), respectively, and integrating, it is found that:

$$\begin{cases} K_{Ic}^U = f(l_c)\sigma_u \\ K_{Ic}^U = \sqrt{h(l_c)}K_{Ic} \end{cases} \tag{6}$$

where

$$f(l_c) = \sqrt{\pi\left(\rho+2l_c\right)}/2 \tag{7}$$

and

$$h(l_c) = \frac{l_c}{\int_0^{l_c}\left[1+\left(\frac{\rho}{5a}\right)^{1.82}\right]^{-0.549}\mathrm{d}a} \tag{8}$$

After some analytical manipulations, system (6) can be rewritten as

$$\begin{cases} \dfrac{\sqrt{h(l_c)}}{f(l_c)} = \dfrac{\sigma_u}{K_{Ic}} \\ K_{Ic}^{U} = \sqrt{h(l_c)}K_{Ic} \end{cases} \tag{9}$$

Once the material properties and the radius are known, the first equation in (9) provides the value of the critical length l_c, which must then be inserted into the second equation of (9) to get the apparent fracture toughness K_{Ic}^{U}.

4. FFM predictions and discussion of results

The coupled FFM criterion expressed by system (9) is now applied to experimental results. It is important to underline that FFM requires the values of the material properties to be known. The estimations of both the tensile strength σ_u and the fracture toughness K_{Ic} obtained experimentally are reported in Table 2. Nevertheless, the value of σ_u cannot be implemented directly to get accurate FFM predictions, since it describes the behavior of plain specimens which failed by involving huge plastic deformations before failure. Thus, in the following σ_u will be replaced by σ_f, which can be interpreted as the microstructural critical fracture stress. Note that i) a similar procedure is also generally adopted for polymers (Taylor 2007, Sapora et al. 2015) due to the presence of micro-cracks/defects and crazing phenomena affecting the strength for un-notched specimens; ii) the fracture stress σ_f was also invoked in Tetelman equations (Wilshaw et al. 1968, Alkin and Tetelman 1971), which were implemented to describe the inversion of behavior between HTA and CTA notched samples (Ritchie et al. 1976).

The implemented values of σ_f reported in Table 2 were obtained by means of a fitting procedure on FFM predictions. Estimations on σ_f for HTA microstructures are smaller than those of CTA ones, reflecting the fact that HTA treated tensile specimens had showed a lower elongation to fracture than CTA ones. The ratio σ_f/σ_u is comprised in the range 1.6-2.1 as it concerns HTA steels, whereas it grows up to 3-4 as it regards CTA steels. Interestingly, A-steel and B-steel (which present the same inclusion content) show nearly the same value of σ_f, whereas that of C-steel is higher for both CTA and HTA samples.

Table 2. Material properties of the steels as in the as-quenched condition from CTA or HTA.

Steel	K_{Ic}(MPa m$^{0.5}$)	σ_u (Mpa)	d_{gs} (μm)	σ_f (MPa)	l_c (μm)
A (CTA)	43	2060	20	6500	28
B (CTA)	43	2110	34	6300	29
C (CTA)	42	2235	18	9000	17
A (HTA)	74	1980	250	3500	286
B (HTA)	54.5	1930	215	3750	134
C (HTA)	47.5	1965	200	4100	83

FFM predictions are reported in Figs. 3, 4 and 5 for A-steel, B-steel and C-steel, respectively. The results are in good agreement with experimental data, although the accuracy decreases for the largest root radii. This is not so surprising, since if the notch radius is not negligible with respect to the notch depth (2 mm for Charpy V-type bars), the expressions (3) and (5) are not apt to describe accurately the stress field function and the SIF function, respectively. FFM predictions could be improved in this case by consider higher order terms in the above asymptotic expressions or by carrying out a finite element analysis. It is also interesting to mention that as ρ increases, involving higher failure loads, the level of constraint can reduce as plastic zones become larger (Taylor 2007).

Eventually, it is interesting to compare the critical crack advance l_c (or characteristic length), which represents the second unknown of system (9) with the austenitic grain size. Since l_c is a structural parameter, it depends both on the material properties and the radius (Sapora et al. 2015). Neglecting the dependence of the radius, its values are

reported in Table 2. For CTA steel there is a good correspondence with the grain size d_{gs}. For HTA steel l_c reflects the coarse grained structure, at least from a qualitative point of view.

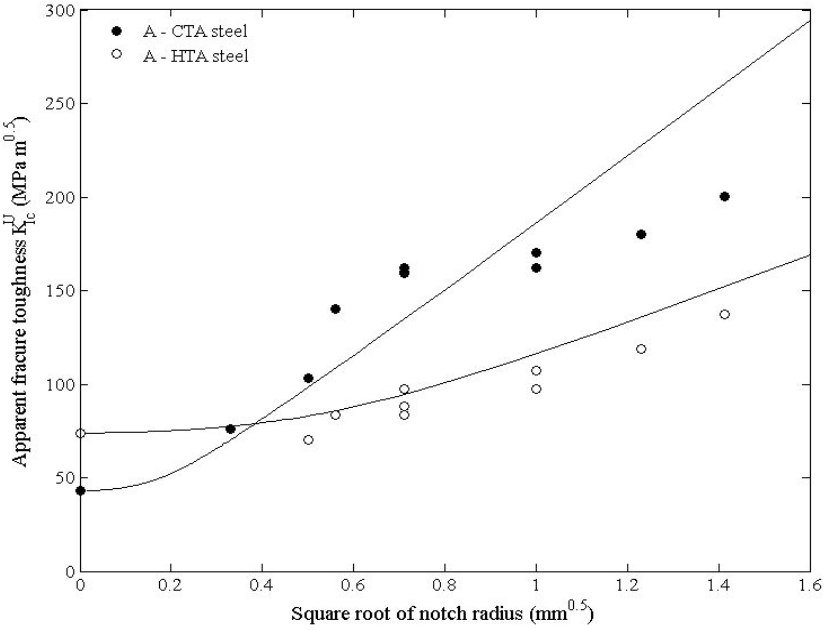

Fig. 3. A-steel: FFM predictions on experimental data carried out in Firrao et al.(1982)

5. Conclusions

High temperature austenitizing (HTA) at 1200 °C of high strength low alloy steels has been introduced more than 40 years ago. In the as-quenched state, it offers interesting features; if the austenitic grain size is elevated to about 250 μm from the usual 20 μm size, an almost double increase of the fracture toughness (K_{Ic}) in respect to conventional temperature austenitizing (CTA) ensues. Yet, Charpy-V notch absorbed impact energies are lower after HTA than after CTA, as it has long been known. Moreover, HTA treated tensile specimens show a lower elongation to fracture than CTA ones.

Detailed fractographic analysis on AISI 4340 steel slow bend tested specimens, with notch root radii varying from almost nihil to 2 mm, showed that both HTA and CTA sharp notch specimens all failed by brittle intergranular fracture, as well as HTA blunt notch specimens. Instead, CTA blunt notch specimens initially failed by plastic instability along logarithmic spirals of a slip line field emanating at some distance from the notch centerline. The betterment of the fracture toughness after HTA was attributed to a large characteristic distance upon which in coarse grained prior austenitic structures the local stress has to be larger than the fracture stress. Such a distance is very small in fine grained structures. By comparing 4340 steel samples with different S and P content, it was seen that higher cleanness steels again show a visible betterment of J_A for as-quenched blunt notch CTA specimens, but not in the case of HTA ones, which continued to fail in a brittle intergranular manner, thus substantiating the idea that the former ones fail by the achievement of a limiting strain at the notch controlling parameter, the latter ones, instead, by a microstructural fracture stress which is adversely affected by the large prior austenitic grain size caused by HTA.

The behavior of HTA and CTA steel samples was analyzed by means of the coupled FFM criterion in terms of brittle macroscopical fracture. In order to implement the approach, two material properties are necessary: i) the fracture toughness, which had been evaluated experimentally; ii) the material strength, which was derived through a fitting procedure since that estimated by tests had been affected by large plastic deformations of plain samples. Good predictions were generally observed, except for very large radii for CTA samples. It was also observed a good

correlation between the FFM crack advance (or characteristic length) and the austenitic grain size.

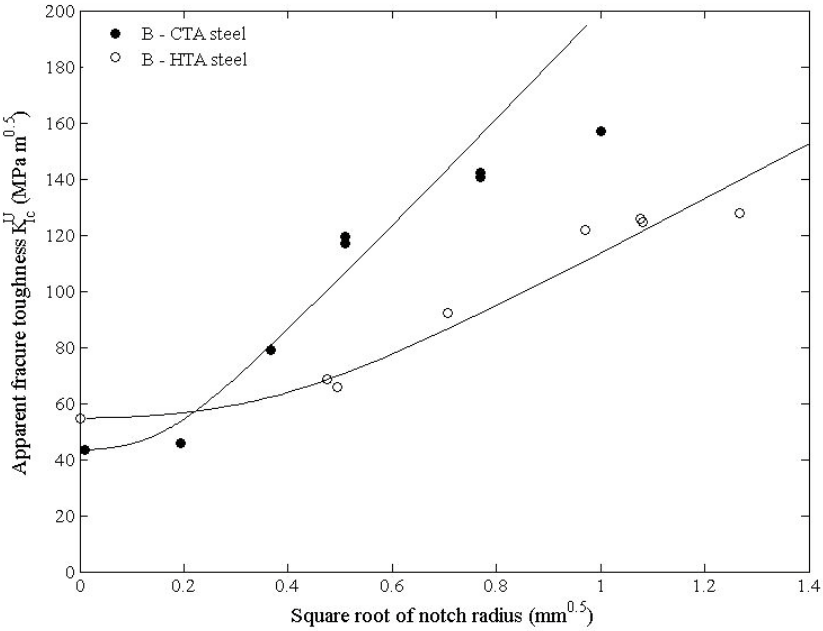

Fig. 4. B-steel: FFM predictions on experimental data carried out in Firrao et al.(2015)

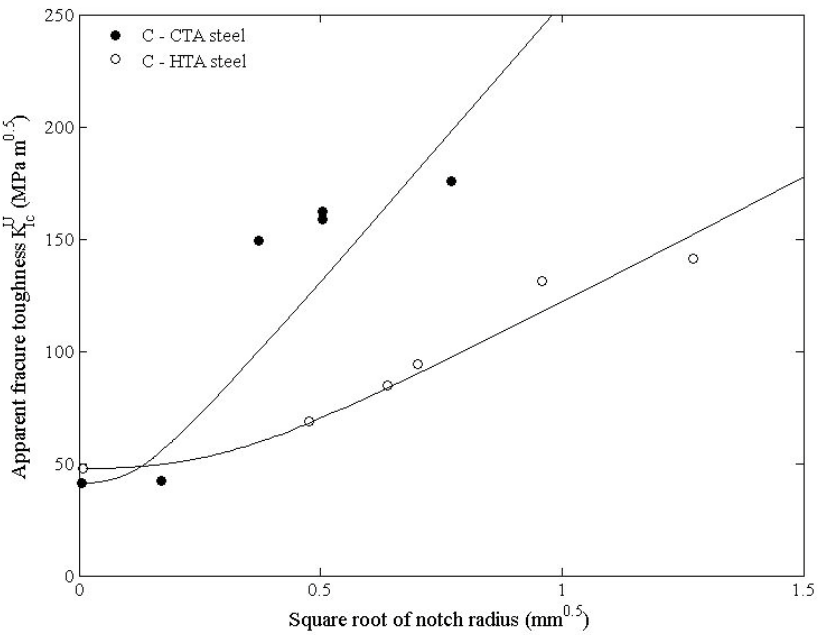

Fig. 5. C-steel: FFM predictions on experimental data carried out in Firrao et al.(2015)

References

Alkin, J.M, Tetelman, A.S., 1971. Relation between K_{Ic} and microscopic strength for low alloy steels. Engineering Fracture Mechanics 3,151-67.

Bashchenko, A.P., Mel'nichenko, N.D., 1969. Metallovedenie i Term. Obrabot. Metallov, 12, 24-27.

Carpinteri, A., Cornetti, P. and Sapora, A., 2012. A finite fracture mechanics approach to the asymptotic behavior of U-notched structures, Fatigue&Fracture of Engineering Materials&Structures 35, 451–457.

Firrao, D., Begley, J.A., Silva, G., De Benedetti, B., Roberti, R., 1982. The influence of notch root radius and austenitizing temperature on fracture appearance of as-quenched Charpy-V type AISI 4340 steel specimens. Metallurgical Transactions A, 13A , 1033-1013.

Firrao, D., Begley, J.A., De Benedetti, B., Roberti, R., Silva, G., 1980. Fracture initiation and propagation at the root of the notch of in as-quenched AISI 4340 steel Charpy V-type bars with varying notch root radii. Scripta Metallurgica 14, 519–524.

Firrao, D., Ugues, D., 2005. Fracture of nitrided and nitrocarburized blunt notch three-point bending die steel specimens. Materials Science and Engineering: A 409, 309-316.

Firrao, D., Matteis, P., Cornetti, P., Sapora, A., 2015. High Temperature Austenitizing of Low Alloy Steels: What Is Left After 40 Years? In: 28th ASM Heat Treating Society Conference, Detroit, Michigan, USA, pp. 64-70.

Glinka, G., 1985. Energy density approach to calculation of inelastic strain-stress near notches and cracks. Engineering Fracture Mechanics 22, 485–508.

Lai, G.Y., Wood, W. E., Clark, R.A., Zackay, V.F., Parker, E.R., 1974. Effect of austenitizing temperature on microstructure and mechanical properties of as-quenched 4340 steel", Metallarurgica Transactions 5, 1663-1670.

Ritchie, R.O., Francis, B., Server, W.L., 1976. Evaluation of toughness in AISI 4340 steel austenitized at low and high temperature. Metallurgical Transactions A.7A, 831-838.

Roberti, R., Silva, G., De Benedetti, B., Firrao, D., 1978. Influenza di un trattamento termico di austenitizzazione ad alta temperature sulle caratteristiche di tenacità di un acciaio AISI 4340 allo stato di piena tempra, La Metallurgia Italiana 70, 449-475.

Sapora, A., Cornetti, P., Carpinteri, A. 2014. Cracks at rounded V-notch tips: an analytical expression for the stress intensity factor, International Journal of Fracture 187, 285–291.

Sapora, A., Cornetti, P., Carpinteri, A., Firrao, D., 2015. An improved Finite Fracture Mechanics approach to blunt V-notch brittle fracture mechanics: Experimental verification on ceramic, metallic and plastic materials. Theoretical and Applied Fracture Mechanics 78, 20–24.

Taylor, D., 2007. The Theory of Critical Distances: A New Perspective in Fracture Mechanics. Elsevier, Oxford, UK.

Wilshaw, T.R., Rau, C.A. , Tetelman, A.S., 1968. A general model to predict the elastic-plastic stress distribution and fracture strength of notched bars in plane strain bending. Engineering Fracture Mechanics 1, 191-211.

Zackay, V.F., Parker, E.R., Goolsby, R.D., Wood, W.E., 1972. Untempered ultra-high strength steels with high fracture toughness, Nature-Physical Science 236, 108-109.